Research Square

Preprints are preliminary reports that have not undergone peer review.
They should not be considered conclusive, used to inform clinical practice,
or referenced by the media as validated information.

# Jatrorrhizine suppresses high-fat diet-associated colorectal cancer by modulating the ATX-LPA-LPAR- MAPK axis to regulate glycerophospholipid metabolism

**Zhiyu Li**
Nanjing University of Chinese Medicine
**Yingjie Gao**
Nanjing University of Chinese Medicine
**Ziwen Li**
Nanjing University of Chinese Medicine
**Shuhong Zeng**
Nanjing University of Chinese Medicine
**Luhua Wu**
Nanjing University of Chinese Medicine
**Wen Zhang**
Nanjing University of Chinese Medicine
**Songling Wang**
Nanjing University of Chinese Medicine
**Haiyan Peng**
phy7073@163.com
Nanjing University of Chinese Medicine
**Weixing Shen**
Nanjing University of Chinese Medicine

**Research Article**

**Keywords:** Jatrorrhizine, colorectal cancer, high-fat diet, glycerophospholipid metabolism, ATX-LPA-LPAR

**Posted Date:** May 22nd, 2026

**DOI:** https://doi.org/10.21203/rs.3.rs-9543581/v1

**License:** This work is licensed under a Creative Commons Attribution 4.0 International License.
Read Full License

**Additional Declarations:** No competing interests reported.

# Jatrorrhizine suppresses high-fat diet-associated colorectal cancer by modulating the ATX-LPA-LPAR-MAPK axis to regulate glycerophospholipid metabolism

ZhiYu-Li[1,2,a], YingJie-Gao[1,2,a], ZiWen-Li[1,2], ShuHong-Zeng[1,2], LuHua-Wu[1,2], Wen-Zhang[1,2], SongLing-Wang[1,2], HaiYan-Peng[1,2,*], WeiXing-Shen[1,2.3. *]

[1]The First Clinical College, Nanjing University of Chinese Medicine, Nanjing 210023, Jiangsu, China

[2]The Affiliated Hospital of Nanjing University of Chinese Medicine, Nanjing 210023, Jiangsu, China

[3]Jiangsu Collaborative Innovation Center of Traditional Chinese Medicine Prevention and Treatment of Tumer, Nanjing 210023, Jiangsu, China

a ZhiYu-Li and YingJie-Gao contributed equally to this work.

*Correspondence should be addressed to HaiYan-Peng and WeiXing-Shen: phy7073@163.com, weixingshen@njucm.edu.cn.

**Abstract**

High-fat diet (HFD) intake is positively correlated with the incidence of colorectal cancer (CRC). It drives CRC through complex mechanisms, yet clinical treatments remain limited, necessitating new strategies. Modern pharmacological studies show that jatrorrhizine (JAT) possesses various biological activities, including antibacterial, antiinflammatory, antiobesity, lipid-lowering, and antitumor effects. Using in vitro and in vivo models of HFD-associated CRC, we found that JAT partially reversed the HFD-induced aggravation of CRC both in vitro and in vivo. Untargeted metabolomics revealed that JAT attenuated the metabolic reprogramming of glycerophospholipid metabolism (GPL metabolism) in HFD-fed CRC model mice, particularly by affecting the metabolite lysophosphatidic acid (LPA). Transcriptomic analysis of cells indicated that JAT regulated the expression of GPL metabolism-related genes in CT26 cells stimulated by an adipocyte-enriched microenvironment. Using techniques such as molecular docking, immunohistochemistry, and ELISA, we demonstrated both in vitro and in vivo that JAT downregulates LPA, its primary biosynthetic enzyme autotaxin (ATX), and the LPA receptor lysophosphatidic acid receptor 2 (LPAR2). Further cellular experiments demonstrated that JAT

promotes ATX degradation via ubiquitination, decreasing the extracellular LPA. The sustained suppression of ligand (LPA) signalling subsequently suppresses LPAR2 transcription. LPAR2 overexpression experiments revealed that JAT inhibits the activation of p-p38MAPK and p-ERK1/2 mediated by LPAR2, thereby suppressing tumour cell proliferation and migration. In summary, JAT treatment partially restores GPL metabolic reprogramming through the ATX-LPA-LPAR2-MAPK axis, thereby inhibiting CRC progression and demonstrating therapeutic potential against HFD-associated CRC.

**Keywords:** Jatrorrhizine; colorectal cancer; high-fat diet; glycerophospholipid metabolism; ATX-LPA-LPAR

## 1 Introduction

According to 2023 statistics from the International Agency for Research on Cancer (IARC), colorectal cancer (CRC) is the fourth most commonly diagnosed malignancy and the fifth leading cause of cancer-related mortality globally[1]. Projections indicate that by 2035, the number of HFD-associated deaths will increase by 71.5% and 60% for colon and rectal cancers, respectively [2]. A Western diet, characterized by high intake of fat, red meat, and processed meats, is a well-established risk factor for cancer[3]. The World Cancer Research Fund International presents compelling evidence that limiting high-fat intake is a significant preventative factor for preventing CRC[4]. Studies have confirmed that a high-fat diet (HFD) promotes colorectal tumorigenesis by disrupting adipokines and inducing lipid metabolic reprogramming[5]. Furthermore, cancer-associated adipocytes facilitate CRC progression through the release of free fatty acids (FFAs) and cytokines such as IL-6[6]. With ongoing socioeconomic development, excessive dietary fat consumption has become a prevalent nutritional pattern. Consequently, the prevention and treatment of HFD-associated CRC warrant further in-depth investigation.

Molecular pathways underlying metabolic dysregulation are now recognized as biomarkers for cancer susceptibility and targets for chemopreventive intervention. Emerging research in traditional Chinese medicine (TCM) has revealed that numerous natural compounds exhibit distinct biological effects on bacteria, viruses, tumours, and inflammation. Jatrorrhizine (JAT), a naturally abundant tetrahydroprotoberberine alkaloid, is derived primarily from TCM herbs such as *Tinospora sagittata*, *Corydalis yanhusuo*, *Coptis chinensis*, and *Phellodendron chinense*. Structurally analogous to berberine and classified within the protoberberine group, JAT is traditionally used in TCM to clear

heat, dry dampness, purge fire, and remove toxins. Recent studies have confirmed its antidiabetic, anticancer, antiobesity, and lipid-lowering properties[7,8]. However, the efficacy and mechanisms of JAT against HFD-associated CRC cancer remain unclear.

Therefore, this study utilized an in vivo HFD-fed AOM/DSS-induced colorectal cancer mouse model and an in vitro coculture model of palmitate (PA)-stimulated 3T3-L1 adipocytes with CT26 murine colorectal cancer cells to explore whether JAT can specifically mitigate HFD-associated CRC. Accordingly, the aim of this study was to investigate the effects of Jatrorrhizine on HFD-related colorectal cancer and its underlying mechanisms. These findings may provide experimental evidence and novel strategies for the use of JAT in the prevention and treatment of HFD-associated CRC.

## 2 Materials and Methods

### 2.1 Materials

The materials used are described as follows: 60Kcal% Fat Purified Diet (catalogue no. XTHF60, Xietong Pharmaceutical Co., Ltd., Nanjing, China); irradiation sterilization experiment mouse maintenance diet (catalogue no. XTI01WC-009, Xietong Pharmaceutical Co., Nanjing, China); Jatrorrhizine (Chengdu Herbpurify Co., Ltd., China); sulfasalazine (SASP, catalogue no. HY-14655, MedChemExpress, USA); azoxymethane (AOM, catalogue no. A5486, Sigma–Aldrich, USA); dextran sulphate sodium salt (DSS, catalogue no. 160110, MP Biomedicals, USA); Amplex Red Triglyceride Assay Kit (catalogue no. S0219S, Beyotime, China); ENPP2/ATX antibody [1F8] (catalogue no. ab77104, Abcam, UK); EDG4 (LPAR2) antibody (catalogue no. PA5-102074, Thermo Fisher, USA); phospho-p38 MAPK (Thr180/Tyr182) (catalogue no. 4511T, Cell Signaling Technology (CST), USA); p38 MAPK (catalogue no. 9212S, CST, USA); phospho-ERK1/2 (Thr202/Tyr204) antibody (catalogue no. 4370T, CST, USA); ERK1/2 antibody (catalogue no. 4695T, CST, USA); β-actin antibody (catalogue no. 4970T, CST, USA); GAPDH antibody (catalogue no. 5174T, CST, USA); β-Tubulin antibody (catalogue no. 2128T, CST, USA); anti-rabbit IgG (catalogue no. ab205719, 1:5000, Abcam, USA); anti-mouse IgG (catalogue no. ab205719, 1:5000, Abcam, USA); interleukin-1 beta (IL-1β) ELISA kit (catalogue no. ml106733y, Mlbio, Shanghai, China); interleukin-6 (IL-6) ELISA kit (catalogue no. ml098430, Mlbio, Shanghai, China); lysophosphatidic acid (LPA) ELISA kit (catalogue no. CB11163-Mu, COIBO, Shanghai, China); Cell Counting Kit-8 (catalogue no. C0038, Beyotime, China); cycloheximide (CHX, catalogue no. HY-12320, MedChemExpress (MCE), USA); proteasome inhibitor MG132 (catalogue no. HY-13259, MCE, USA); chloroquine (CQ, catalogue no. HY-17589A, MCE, USA);

palmitic acid (catalogue no. HY-N0830, MCE, USA); 5% fatty acid-free bovine serum albumin (catalogue no. HY-D0842A, MCE, USA); CT26 cells (provided by Jiangsu Collaborative Innovation Center of Traditional Chinese Medicine Prevention and Treatment of Tumor); 3T3-L1 Swiss albino mouse embryonic fibroblasts (catalogue no. CL-0006, Procell Life Science & Technology Co., Ltd. (Pricella), China); medium For 3T3-Swiss albino (mouse embryonic fibroblasts) adipogenic differentiation (catalogue no. PD-034, Pricella, China); Steadypure quick RNA extraction kit (catalogue no. AG21205, accurate biotechnology, China); SYBR Green Premix Pro Taq HS qPCR Kit (catalogue no. AG11762, Accurate Biotechnology, China)

**2.2 Animals and treatment**

Eight-week-old male C57BL/6 mice were purchased from GemPharmatech Co., Ltd. All the mice were housed in the Laboratory Animal Center of Nanjing University of Chinese Medicine under controlled environmental conditions (20±2°C, 50±5% humidity, 12-hour light/dark cycle) and fed either a normal chow diet or a high-fat diet. After 7 days of acclimatization, using a random number table, the mice were randomly divided into the following groups (n=9 per group): negative control (CTRL), high-fat diet model (HFD), AOM/DSS model (CRC), high-fat diet + AOM/DSS (HFD+CRC), AOM/DSS + low-dose JAT (CRC+JAT-L), AOM/DSS + high-dose JAT (CRC+JAT-H), high-fat diet + AOM/DSS + low-dose JAT (HFD+CRC+JAT-L), high-fat diet + AOM/DSS + high-dose JAT (HFD+CRC+JAT-H), AOM/DSS + sulfasalazine (CRC+SASP), and high-fat diet + AOM/DSS + sulfasalazine (HFD+CRC+SASP). The mice in the CTRL and HFD groups received normal drinking water, while those in the other groups were subjected to CRC modelling via the AOM/DSS protocol. Specifically, 10 mg/mL/kg AOM was intraperitoneally administered on day 1 and day 5 of the first week, followed by three cycles of 2% DSS in the drinking water (1 week of DSS + 2 weeks of normal water per cycle). The HFD groups were maintained on a HFD throughout. The CRC+HFD+JAT-L and CRC+JAT-L groups received JAT (100 mg/kg/day), whereas the HFD+CRC+JAT-H and CRC+JAT-H groups received JAT (200 mg/kg/day). The CRC+SASP and HFD+CRC+SASP groups were administered sulfasalazine (200 mg/kg/day). All treatments were delivered via oral gavage six times weekly for 10 consecutive weeks. The remaining groups received 0.1 mL/10 g of 0.9% sodium chloride solution according to the same administration protocol.

**2.3 Histological staining and HE**

Colonic tissues were rolled into Swiss rolls, fixed in 10% paraformaldehyde solution, and embedded in paraffin following standard protocols. Serial 5 μm thick sections were prepared using

a microtome. The tissue sections were dewaxed with xylene, rehydrated through a graded ethanol series, and stained with haematoxylin and eosin (H&E) for histopathological analysis. Pathological alterations in the colonic tissues were examined under a light microscope (XD-202, Leica), and H&E-stained images were captured using a camera (DP27, Olympus).

**2.4 Nontargeted metabolomics**

Blood samples collected from mice were transferred to EP tubes and centrifuged at 3000 rpm for 20 min at 4°C. The supernatant (serum) was aliquoted into fresh EP tubes, immediately snap-frozen in liquid nitrogen, and stored at −80°C for subsequent serum nontargeted metabolomics analysis. Metabolite analysis was performed on an AB SCIEX Triple TOF 6600 by Gene Denovo Biotechnology Co., Ltd. (Guangzhou, China).

**2.5 Immunohistochemistry, IHC**

Three samples per group were processed for immunohistochemistry. The tissue sections were baked, deparaffinized in xylene, and rehydrated through a graded ethanol series. Antigen retrieval was carried out using citrate buffer at pH 6.0 with heating in a microwave at 95°C for 20 minutes, followed by cooling and rinsing in PBS. Endogenous peroxidase activity was blocked by incubation with 3% $H_2O_2$ for 20 minutes in the dark. The sections were then incubated with normal goat serum for 25 minutes at room temperature, followed by an overnight incubation at 4°C with primary antibodies against Ki67, ATX, and LPAR2 at a dilution of 1:200. After the samples were washed with PBS, an HRP-conjugated secondary antibody was applied at a 1:500 dilution and incubated for 2 hours at room temperature. Detection was performed using DAB visualization with haematoxylin counterstaining. Finally, the sections were dehydrated, cleared in xylene, and coverslipped. Three random fields per sample were imaged and analysed using ImageJ software.

**2.6 Adipocyte culture and coculture system**

The murine colon carcinoma cell line CT26 was obtained from the cryopreserved stock of our laboratory and cultured in Dulbecco's modified Eagle’s medium (DMEM) supplemented with 10% foetal bovine serum (FBS) and 1% penicillin–streptomycin. 3T3-L1 mouse embryonic fibroblasts (Pricella) were maintained in a specific growth medium for 3T3-L1. Both cell lines were incubated at 37°C in a humidified atmosphere containing 5% $CO^2$. For adipogenic differentiation, 3T3-L1 preadipocytes were seeded in 6-well, 12-well, or 96-well plates containing 0.4 μm Transwell inserts

and induced using Pricella's adipogenic differentiation protocol for 7–9 days until >90% of the cells differentiated into mature adipocytes. A palmitate (PA) stock solution (80 mM) was prepared by dissolving PA in 0.1 mol/L NaOH at 70°C with agitation. The stock was then complexed with 5% fatty acid-free bovine serum albumin (BSA) in serum-free DMEM to generate a 5 mM PA working solution. Freshly prepared 0.6 mM PA working solution was applied to 3T3-L1 adipocytes for 24 h. Controls received DMEM supplemented with 5% BSA. For coculture experiments, mature/palmitate-treated mature adipocytes and CT26 cells were placed in the upper/lower chambers of Transwell inserts with DMEM for 48 h. CT26 cells cocultured with mature adipocytes were designated the Mature adipocyte-Conditioned Medium (MCM) group, while those cocultured with palmitate-treated mature adipocytes were defined as the Palmitate-treated mature adipocyte-Conditioned Medium (PCM) group[9].

**2.7 Oil Red O staining and triglyceride (TG) assays**

Lipid accumulation in 3T3-L1 cells was assessed via microscopic visualization with Oil Red O staining and quantitative analysis using a microplate reader. The cells were fixed with 4% paraformaldehyde for 10 min, stained with Oil Red O working solution (prepared at a 3:2 ratio of stock solution to diluent) for 20 min, washed, and imaged under a microscope. The intracellular triglyceride content was measured following the manufacturer's protocol. Briefly, the samples were sonicated on ice (4°C) using an ultrasonic cell crusher (Qsonica Q700 Newtown, CT, USA). Reagents were sequentially added according to the manufacturer's instructions, and the absorbance at 520 nm was quantified using a microplate reader.

**2.8 Cell viability**

The half-maximal inhibitory concentration (IC50) of JAT on CT26 cells was determined via a Cell Counting Kit-8 (CCK-8) assay. CT26 cells ($1\times10^4$/well) were seeded in 96-well plates, treated with JAT (0–400 μmol/L) for 24 h, incubated with 10 μL of CCK-8 reagent (37°C, 2 h), and analysed at 450 nm using a microplate reader (Bio-Rad).

For coculture experiments, CT26 cells ($1\times10^3$/well) were grouped into the following groups: CON (DMEM control), MCM (mature adipocyte-conditioned medium), PCM (palmitate-treated mature adipocyte-conditioned medium), and JAT-treated groups. After 48 h of coculture, the 3T3-L1 adipocytes in the upper chambers were removed. Each group was treated with JAT (25 – 200 μ

mol/L) or left untreated for 24 hours, followed by the aforementioned CCK-8 protocol. The cell viability of stable LPAR2-overexpressing CT26 transfectants was measured using a CCK-8 assay following the same protocol as previously described.

**2.9 Cell proliferation detection via a colony formation assay**

CT26 cells ($1\times10^3$/well) were seeded in 6-well plates and grouped into the following groups: CON, MCM, PCM control, and JAT-treated groups. After 48 h of coculture, the upper chambers were removed. The PCM-treated groups were exposed to JAT (25–100 μmol/L) for 7 days. Colonies containing >50 cells were defined as single clones. The cells were fixed and stained with 0.1% crystal violet (0.1 g in 100 mL of methanol) for 30 min, air-dried, and imaged. Stable LPAR2-overexpressing CT26 transfectants were subjected to a colony formation assay under identical experimental conditions as previously detailed.

**2.10 Scratch wound healing assay**

CT26 cells were seeded in 6-well plates and subjected to groups and coculture procedures as previously described. Scratch wounds were generated using a sterile 10 μL pipette tip. Images were captured at 0 h and 24 h (three fields per time point) after JAT treatment (50 and 100 μmol/L) in the PCM-treated groups. The cell migration rate was calculated via ImageJ as follows: (0 h–24 h)/scratch area at 0 h × 100%. Stable LPAR2-overexpressing CT26 transfectants were subjected to a wound healing assay using an identical protocol as previously described.

**2.11 Metatranscriptome sequencing**

Total RNA was extracted from control and treated cells using TRIzol reagent. PCR products were purified with the AMPure XP system, and library quality was assessed on an Agilent Bioanalyzer 4150. Sequencing was performed on an Illumina NovaSeq 6000/MGISEQ-T7 platform. Metatranscriptomic sequencing and analysis were conducted by Applied Protein Technology (Shanghai, China).

**2.12 Western blotting (WB)**

Total protein was extracted from cells using RIPA lysis buffer containing a phosphatase inhibitor and protease inhibitor cocktail. Protein concentrations were quantified via a BSA standard curve. The proteins were separated by SDS–PAGE and transferred to PVDF membranes.

The membranes were blocked with Rapid Blocking Buffer or 5% BSA for 10 h or 1 h. Subsequently,

the membranes were incubated sequentially with two primary antibodies raised in the same host species (e.g., rabbit): first, the anti-loading control antibody (e.g., anti-GAPDH) was added for 2 hours at room temperature, followed by the anti-target protein antibody for 2 hours at room temperature. This mixture was then incubated with the entire membrane. After being washed, the membranes were incubated with horseradish peroxidase (HRP)-conjugated anti-mouse/anti-rabbit secondary antibodies for 1 h at room temperature. The protein bands were visualized using a hypersensitive chemiluminescence imaging system (Tanon, China).

**2.13 Quantitative PCR analyses and qPCR**

Total RNA was extracted using a SureTrace Quick RNA Extraction Kit, after which cDNA was synthesized according to the manufacturer's protocol. Relative mRNA expression levels were quantified using the 2^-ΔΔCQ method with the following qPCR primers. Amplification was performed using a SYBR Green Premix Pro Taq HS qPCR Kit.

Table 1 Primer sequences

| Genes | F | R |
|---|---|---|
| ENPP2 | CTGTCGGTGTGACAACCTATGTA | TTGGTAGTTGGTACAGCAGTCTC |
| LPAR2 | F:GTCCCACAGCTCCAGTCATT | TGGATTTTCCCTCTGCACCC |
| MAPK14 | F:GATGAGCCTGTTGCTGACCCTTA | TGGTGGCACAAAGCTGATGAC |
| ERK-1 | CAGCTCAACCACATTCTAGGTA | TCAAGAGCTTTGGAGTCAGATT |
| ERK-2 | ATCTCAACAAAGTTCGAGTTGC | GTCTGAAGCGCAGTAAGATTTT |
| GAPDH | TGTGTCCGTCGTGGATCTGA | TTGCTGTTGAAGTCGCAGGAG |

**2.14 ELISA**

Serum samples and cell culture supernatants (from WB experiments) were collected in sterile tubes and centrifuged at 3,000 × g for 20 min at 4°C. The clarified supernatants were carefully collected for subsequent analysis. Levels of IL-6, IL-1β, and LPA in serum, as well as LPA in cell culture supernatants, were quantified using commercial ELISA kits according to the manufacturer's protocols.

**2.15 Molecular docking**

The active component JAT was retrieved in Mol2 format from the Traditional Chinese Medicine Systems Pharmacology Database (TCMSP). Three-dimensional structural models of ATX (UniProt ID: Q13822; AlphaFold model version: AF-Q13822-F1) and LPAR2 (UniProt ID:

Q9HBW0; AlphaFold model version: AF-Q9HBW0-F1) were obtained from the UniProt database (https://www.uniprot.org/). Solvent molecules and nonessential ligands were removed from the protein structures using PyMOL v2.5.4 (Schrödinger LLC). Structures were energy-minimized and converted to PDBQT format for docking compatibility. The CB-Dock2 platform (https://cadd.labshare.cn/cb-dock2/) was employed for blind docking between JAT and target proteins (ATX/LPAR2). Protein–ligand interactions (hydrogen bonds and hydrophobic contacts) were visualized using PyMOL.

**2.16 Stable cell line establishment**

Lentiviral vector construction and packaging were outsourced to Nanjing Keshengjie Biotechnology Co., Ltd., utilizing the murine LPAR2 gene (Gene ID: 53978) cloned and inserted into the pLV3-CMV-LPAR2-3×FLAG-CopGFP-Puro expression cassette. CT26 cells in the logarithmic growth phase were seeded into 24-well plates at a density of $5\times10^4$ cells/well. Upon reaching approximately 30% confluence, the cells were transduced with lentivirus at the predetermined multiplicity of infection (MOI) using either the LPAR2-overexpressing lentivirus (OE-LPAR2) or the empty vector control lentivirus (vector). Stable LPAR2-overexpressing CT26 transfectants were subsequently selected and established via puromycin resistance screening.

**2.17 Data analysis**

All experiments were independently repeated three times. Data are presented as the mean ± standard deviation (SD) and were analysed using GraphPad Prism 9.0 (GraphPad Software, San Diego, CA, USA). Statistical analysis was performed using Student's t test for comparisons between two groups and one-way ANOVA followed by Bonferroni post hoc correction for multiple comparisons. A p value $< 0.05$ was considered to indicate statistical significance.

**3 Results**

**3.1 JAT treatment inhibits tumour progression in CRC and HFD-related CRC model mice**

To investigate the effects of JAT on HFD-associated colorectal tumorigenesis, AOM/DSS-treated BALB/c mice were fed a normal diet or a HFD (Fig. 1A). After the 10-week intervention, the survival rates were 100% (CTRL), 100% (HFD)77% (CRC), 55% (HFD+CRC), 88% (CRC+SASP), 100% (HFD+CRC+SASP), 88% (CRC+JAT-L), 100% (CRC+JAT-H), 88%

(HFD+CRC+JAT-L), and 100% (HFD+CRC+JAT-H) (Fig. 1B). During the DSS treatment period, body weight decreased rapidly in both the HFD+CRC group and the CRC group. The body weights of the HFD+CRC model mice were lower than those of the CRC group mice at week 10, likely because of more rapid tumour progression, whereas the body weights of the JAT-treated mice increased (Fig. 1C). Colorectal length was significantly shorter in CRC and HFD+CRC than in CTRL (HFD+CRC > CRC), but JAT restored length, particularly in HFD+CRC+JAT-H > HFD+CRC+SASP (Fig. 1D, E). Tumours were present in all groups except the CTRL/HFD group, with a greater burden in the HFD+CRC group than in the CRC group. JAT/SASP significantly reduced tumour number and burden; however, compared with CRC+JAT-H, CRC+SASP exhibited greater efficacy, whereas the effects of HFD+CRC+JAT-H and HFD+CRC+SASP were comparable (Fig. 1D, F).

HE staining demonstrated preserved colonic architecture in the CTRL and HFD groups, whereas CRC model mice exhibited glandular disorganization, goblet cell depletion, high-grade intraepithelial neoplasia in tumour crypts, increased mitotic activity, mucosal tumour infiltration, and inflammatory cell infiltration in peritumoral regions, muscularis mucosae, and serosa—pathologies, which were exacerbated in HFD+CRC model mice. JAT and SASP interventions significantly ameliorated these histopathological alterations (Fig. 2A). Molecular profiling confirmed the increased expression of the proliferative marker Ki67 (IHC) and the prognostic biomarkers IL-1β/IL-6 (ELISA) in HFD+CRC and CRC model mice; notably, the expression of these markers was significantly decreased by JAT treatment (Fig. 2B–E). High-dose JAT (JAT-H) exerted the most pronounced therapeutic effects in CRC and HFD+CRC model mice, with efficacy comparable to that of SASP. Consequently, JAT-H was selected for mechanistic investigation.

**3.2 JAT suppresses adipocyte-induced CRC cell proliferation and migration in vitro**

As previously described, for the in vitro experiments, $PA^-$ refers to mature 3T3-L1 adipocytes not treated with palmitic acid, whereas $PA^+$ refers to those that were PA-incubated to artificially generate a hypertrophic state. Compared with those in the $PA^-$ group, lipid accumulation and intracellular triglyceride (TG) levels in the $PA^+$ group were significantly greater. These results demonstrate that PA effectively induces hypertrophy in 3T3-L1 adipocytes, representing a pathological feature of an abnormal adipocyte microenvironment (Fig. 3A-B). JAT inhibited CT26

cell proliferation at subcytotoxic concentrations (25–100 μM) without inducing apoptosis, with IC50 values ranging from 96.56 to 106.2 μM (Fig. 3C). CCK-8 and clonogenic assays revealed that coculture with 3T3-L1 adipocytes promoted the proliferation of CT26 cells. This enhanced proliferation was effectively suppressed by JAT at concentrations of 25, 50, and 100 μM. (Fig. 3D–E). Scratch assays further demonstrated accelerated CT26 migration under coculture conditions, in which JAT treatment significantly suppressed CT26 migration (Fig. 3F).

**3.3 Nontargeted metabolomics revealed changes in metabolites in CRC and HFD+CRC model mice following JAT treatment**

To investigate metabolic disparities between a normal diet-associated CRC and HFD-associated CRC, as well as the changes before and after JAT treatment,LC–MS/MS-based metabolomic profiling of 25 serum samples revealed 1,315 metabolites. Orthogonal partial least squares-discriminant analysis (OPLS-DA) combining positive/negative ion modes (thresholds: VIP >1, $p<0.05$, fold-change ≥2) revealed distinct metabolic clusters, with quality-controlled principal component analysis (PCA) confirming high intragroup reproducibility and significant intergroup separation (Fig. 4A). A clustered heatmap revealed poor correlations between the CRC/HFD+CRC group and the CTRL group, whereas the CRC+JAT and HFD+CRC+JAT groups exhibited a restored correlation with the CTRL group (Fig. 4B). Comparative analysis of differentially abundant metabolites revealed 369 upregulated and 48 downregulated metabolites in the CRC group vs. the CTRL group, and this dysregulation pattern was exacerbated in the HFD+CRC group. Furthermore, compared with the CTRL samples, the HFD+CRC samples exhibited 683 upregulated and 110 downregulated metabolites whose expression was reversed by JAT intervention in the HFD+CRC+JAT (Figure 4C). Notably, the most pronounced metabolic shifts occurred in the HFD+CRC versus HFD+CRC+JAT comparisons, prompting focused investigations of CRC versus HFD+CRC and HFD+CRC versus HFD+CRC+JAT.

On the basis of metabolite identification, compound IDs (C_id) were mapped to the Kyoto Encyclopedia of Genes and Genomes (KEGG) database, with the top 20 enriched pathways (Q-value ordered) revealing shared mechanisms in CRC vs. HFD+CRC and HFD+CRC vs. HFD+CRC+JAT comparisons: lipid metabolism glycerophospholipid (GPL) metabolism, biosynthesis of unsaturated fatty acids, fatty acid elongation/degradation), choline metabolism in

cancer, efferocytosis, biosynthesis of plant secondary metabolites, protein digestion/absorption, and aminoacyl-tRNA biosynthesis (Fig. 4E-F). These pathways mechanistically explain HFD-driven carcinogenesis, whereas JAT intervention reversed these alterations, suggesting that JAT alleviates intestinal tumorigenesis and HFD-associated oncogenesis primarily through modulating lipid/amino acid metabolism. Focusing on the top three pathways (GPL metabolism, choline metabolism in cancer, and efferocytosis), we identified predominant GPL-class metabolites. Subsequent analysis of differential GPL metabolites—including phosphatidylcholines (PC), phosphatidylethanolamines (PE), phosphatidylinositols (PI), platelet-activating factor (PAF), and phosphatidic acid—revealed that the expression of distinct metabolites, such as sn-Glycero-3-phosphocholine, LysoPC(P-18:0/0:0), LysoPC(P-16:0/0:0), LysoPA(22:5/0:0), and LPA(0:0/15:0) showed low expression in CTRL, elevated expression in CRC, further increased expression in HFD+CRC, and reduced expression in JAT-treated groups; conversely, LysoPC(22:4/0:0), LysoPC(22:6/0:0), LysoPC(22:5/0:0), LysoPC(18:1(11Z)), LysoPC(20:2), and LPC(18:1) displayed high expression in the CTRL group , reduced expression in the CRC group, further decreased expression in the HFD+CRC group, and upregulation in the JAT treatment group (Fig. 4D). We specifically identified the metabolites LysoPA (22:5/0:0) and LPA (0:0/15:0) as significantly elevated in the HFD+CRC group compared with those in the CTRL and CRC groups, with JAT effectively reducing the serum levels of these LPA species (Fig. 4G). Given that ATX catalyses the conversion of lysophosphatidylcholine (LPC) to LPA—accounting for >80% of extracellular LPA biosynthesis—and that LPA exerts diverse biological functions through binding to LPA receptors (LPAR1-6) [10], we hypothesize that JAT mitigates HFD-associated colorectal cancer via modulation of the ATX-LPA-LPAR axis and its downstream signalling pathways.

### 3.4 Transcriptomics was employed to identify mRNAs that are differentially regulated by JAT in CT26 cells in the adipocyte microenvironment

To investigate the regulatory effects of mature adipocytes and palmitate-treated mature adipocytes on CT26 cell gene expression and to determine whether JAT suppresses CT26 proliferation through GPL metabolism-related gene modulation, we conducted mRNA transcriptome profiling. PCA revealed significant transcriptomic divergence among the four experimental groups (Fig. 5A). With thresholds of $|\log_2 FC| > 1$ and $p < 0.05$, JAT treatment

differentially regulated 3,091 genes in the CON group comparison, 3,392 genes in the MCM group comparison, and 2,974 genes in the PCM group comparison, while PCM modulated 322 genes in the CON group comparison (Supplementary Data). Volcano plots were constructed to visualize the distribution and directional regulation of differentially expressed genes in the PCM group versus the JAT-treated group (Fig. 5B). KEGG analysis revealed that the pathways predominantly enriched in JAT in CT26 cells within the adipocyte microenvironment included glycerophospholipid metabolism, cell cycle, choline metabolism in cancer, nucleotide metabolism, sphingolipid metabolism, inositol phosphate metabolism, aminoacyl-tRNA biosynthesis, steroid biosynthesis, and arginine and proline metabolism (Fig. 5C). Notably, some of these pathways overlapped with those identified in the previous serum metabolomics analysis of mice. Subsequent analysis of GPL metabolism-associated genes revealed key families: phospholipase A2 (PLA2), diacylglycerol kinase (DGK), lysophospholipid acyltransferases (LPCAT/LCLAT), phospholipase D (PLD), phosphatidic acid phosphatases (PLPP), and lysophosphatidic acid receptors (LPAR) (Fig. 5D).

**3.5 HFD consumption and the adipocyte microenvironment activate the ATX-LPA-LPAR-MAPK signalling axis in CRC model mice and CT26 cells, whereas JAT treatment inhibits this pathway**

Molecular docking analysis was employed to investigate the interactions between JAT and target proteins. The ATX-JAT complex exhibited a Vina score of -9.1, indicating that the high binding affinity was primarily mediated by π–π stacking interactions, whereas the LPAR2-JAT complex achieved a Vina score of -8.6, with hydrogen bonding as the dominant force (Fig. 6A). ELISA and IHC analyses of murine colonic tissues revealed that serum ATX and LPA levels were specifically elevated in the HFD+CRC group compared with those in the CRC group, whereas JAT intervention downregulated ATX and LPA expression in the colonic tissues of both the CRC and the HFD+CRC groups. Similarly, coculture with 3T3-L1 cells increased LPA levels in the supernatant of CT26 cells, and JAT treatment suppressed this increase. (Fig. 6B), which aligns with the metabolomic findings. The results of IHC staining revealed upregulated ATX and LPAR2 expression in the HFD+CRC group compared with the CRC group. Both low- and high-dose JAT significantly reduced the positive staining rates of ATX and LPAR2 in tumour tissues compared with those in the

model groups (Fig. 6C).

Subsequently, we used an in vitro model to verify whether HFD-associated CRC activates the ATX－LPA－LPAR2－MAPK signaling pathway in CT26 cells. we examined the protein and mRNA expression of this pathway using WB and qRT–PCR. Consistent with the in vivo results, the protein levels of ATX, LPAR2, p-P38MAPK, and p-ERK1/2 were elevated in the MCM and PCM groups but were reduced following JAT treatment (Figure 6 D). The mRNA expression levels of LPAR2, P38MAPK, ERK1, and ERK2 largely mirrored the protein expression trends (Figure 6E). However, the level of intracellular ATX (ENPP2) mRNA expression decreased below the limit of detection. These results are consistent with those of transcriptomic data and external database validations (Human Protein Atlas, https://www.proteinatlas.org/), which may be related to posttranslational modifications or mRNA stability.

**3.6 JAT inhibits the LPAR2-activated MAPK signalling pathway and directly promotes the proteasomal degradation of ATX**

To investigate whether JAT inhibits LPAR2, thereby reducing p38 MAPK and ERK1/2 phosphorylation, we established stable LPAR2 (OE-LPAR2) overexpression in CT26 cells. Both qPCR and WB analyses demonstrated that the overexpression levels in the OE-LPAR2 group were approximately 2.3-fold and 2-fold greater, respectively, than those in the vector group, confirming successful construction. (Figure 7 A, B). Subsequent functional assays, including CCK-8, colony formation, and wound healing assays, demonstrated that compared with the vector control group, the OE-LPAR2 group exhibited significantly enhanced cellular proliferation and migration. Compared with those in the PCM group, proliferation and migration in the OE-LPAR2 group were comparable, and no significant difference was observed between the OE-LPAR2 group and the OE-LPAR2 group treated with JAT. These findings indicate that LPAR2 overexpression promotes CT26 cell proliferation and migration, suggesting that this gene mimics the protumorigenic effects of the adipocyte microenvironment. Furthermore, LPAR2 overexpression reversed the antiproliferative and antimigration effects of JAT on CT26 cells (Figure 7 C–E). WB analysis revealed that JAT treatment failed to downregulate p-p38 MAPK and p-ERK1/2 expression in OE-LPAR2 CT26 cells but still downregulated ATX expression. These findings suggest that JAT intrinsically downregulates ATX expression independent of LPAR2 (Figure 7F). We further investigated the degradation

pathway of the ATX protein mediated by JAT. CT26 cells were cocultured with palmitate-treated mature adipocytes for 48 hours, and the upper chambers were removed and treated with CHX (50 μg/mL), MG132 (20 μmol/L), or CQ (20 μmol/L) in the presence of 100 μM JAT for 24 hours. WB analysis of ATX protein expression levels was conducted to evaluate proteasome-mediated degradation. The results revealed that MG132 reversed the inhibitory effect of JAT on ATX expression, whereas CQ did not, indicating that JAT modulates ATX degradation via the ubiquitin–proteasome pathway (Figure 7G).

## 4 Discussion

The relationship between a HFD and cancer has garnered increasing attention, with numerous studies indicating that a HFD increases the risk of CRC [11,12]. It is well established that a HFD leads to obesity, a condition recognized by the World Cancer Research Fund International as a risk factor for CRC, on the basis of compelling evidence [4]. Consequently, there is a pressing need for effective agents to prevent and treat HFD-associated CRC. The dysregulation of metabolites induced by a HFD represents a key pathological feature in promoting colorectal tumorigenesis [5]. Studies have revealed heterogeneity in the lipidome of CRC patients compared with that of healthy individuals, suggesting that disturbances in GPLs may be involved in tumour initiation and progression [13–15]. While a limited number of agents have been reported to ameliorate HFD-associated CRC[16,17], the efficacy of JAT in its prevention and treatment remains unclear.

In this study, an in vivo model of HFD-associated colorectal cancer was established by feeding C57BL/6J mice a HFD combined with AOM/DSS induction. For in vitro experiments, a coculture system of 3T3-L1 adipocytes and mouse CT26 colorectal cancer cells was used. A HFD leads to obesity and abnormal adipokine secretion. During the adipogenic differentiation of 3T3-L1 cells, numerous adipokines are activated, resulting in substantial alterations in the levels of intracellular lipid metabolites—particularly TG, DG, SM, Cer, PI, PC, PE, etherPE, etherPC, LPC, and LPE [18]. PA was used to induce adipocyte hypertrophy, which significantly promoted triglyceride accumulation in 3T3-L1 adipocytes and triggered inflammatory responses along with reduced expression of tumour suppressor genes [19–21]. These changes mirror the adipokine dysregulation and inflammation induced by a HFD, thus providing a pathophysiological basis for utilizing the

adipocyte microenvironment as a relevant in vitro model of HFD-induced colorectal cancer. In summary, we believe that the animal and cellular models used in this study effectively mimic human HFD-associated CRC.

Here, we demonstrate that a high-fat diet (HFD) exacerbates AOM/DSS-induced colorectal cancer (CRC) and that coculture with 3T3-L1 adipocytes promotes the proliferation and migration of CT26 cells. JAT treatment prevented and alleviated HFD-driven AOM/DSS-induced CRC and suppressed the proliferation and migration of CT26 cells cocultured with 3T3-L1 adipocytes. Furthermore, metabolomic and transcriptomic analyses revealed that JAT inhibited CRC progression in mice and the proliferation/migration of CT26 cells by modulating pathways related to lipid metabolism, choline metabolism in cancer, and protein digestion and absorption in both HFD-associated CRC model mice and CT26 cells in an adipocyte-enriched microenvironment. Untargeted metabolomics indicated that a HFD induced glycerophospholipid (GPL) metabolic reprogramming. Previous studies have established a close association between aberrant GPL metabolism and cancer progression[22–24]. Specifically, JAT primarily attenuated the abnormally elevated expression of LPA metabolites in the GPL metabolism pathway in HFD-fed CRC model mice. Transcriptomic data further confirmed that JAT could selectively regulate gene families associated with LPA metabolism at the cellular level, including the PLA2, DGK, LPCAT/LCLAT, PLD, PLPP, and LPAR families. To further elucidate how JAT regulates LPA within the GPL metabolic pathway, molecular docking suggested a high binding affinity between JAT and both ATX and LPAR2. IHC, WB, ELISA, and qPCR experiments confirmed that JAT inhibits ATX-LPA-LPAR2 signalling and downstream MAPK signalling in vivo and in vitro. Since LPA induces ATX expression while also acting as a ligand to regulate the transcription of its receptor LPAR, the ATX-LPA-LPAR axis is recognized as a classic positive feedback loop in carcinogenesis [10,25]. Multiple studies have indicated that ATX promotes CRC initiation and progression [26,27]. ATX, encoded by ENPP2, is a secreted lysophospholipase D (lysoPLD) that belongs to the ENPP protein family. It is primarily secreted into the extracellular space. The secretion mechanism involves cleavage of the N-terminal signal peptide and furin-mediated processing of the ATX precursor protein, followed by N-glycosylation at N52, N410, and N524. The modified glycoprotein is then secreted via the classical endoplasmic reticulum–Golgi pathway, where it catalyses the degradation of LPC to

produce LPA[28]. Intermediates or end products of GPL metabolism, such as phosphatidic acid (PA), lysophosphatidic acid (LPA), and free fatty acids, can serve as precursors or intermediates required for tumour growth and proliferation, thereby contributing to tumorigenesis[29]. Both clinical and laboratory evidence suggest that elevated circulating LPA levels can be considered biomarkers for cancer progression[30,31]. LPA receptors (LPARs) are widely expressed in most cell types. The binding of LPA to LPARs activates these receptors, enabling LPA to perform diverse biological functions. Six G protein-coupled LPARs on the cell surface mediate the majority of the effects of LPA. Clinical studies have shown higher LPAR2 mRNA expression in CRC tissues than in adjacent normal tissues[32], and the loss of LPAR2 suppresses intestinal tumorigenesis driven by ApcMin mutation[33]. LPARs are coupled with Gi/o in some cells, leading to inhibition of adenylate cyclase activity and activation of the Ras/mitogen-activated protein kinase (MAPK/ERK) and protein kinase B/Akt pathways. This pathway demonstrates interactive potential and, in turn, regulates cell proliferation, survival, differentiation, and motility[34]. However, this effect has not been validated in colorectal CT26 cells. Therefore, we overexpressed LPAR2 to verify whether the LPAR2 protein can activate MAPK signalling. The overexpression of LPAR2 in CT26 cells promoted CRC cell proliferation and migration and partially reversed the JAT-mediated inhibition of MAPK pathway activation without affecting JAT-mediated suppression of ATX. These findings confirm that the LPAR2 protein indeed activates MAPK signalling in CT26 cells. p38MAPK and ERK1/2, members of the mitogen-activated protein kinase (MAPK) family, can be activated by various stimuli and regulate tumour cell proliferation, migration, and invasion[35]. Furthermore, the addition of the autophagy inhibitor QC under JAT treatment did not inhibit the JAT-induced decrease in ATX protein expression, whereas the addition of the proteasome inhibitor MG132 did. MG132 is a proteasome inhibitor that reversibly inhibits proteasome activity within cells, thereby suppressing protein degradation mediated by the ubiquitin–proteasome system (UPS). These findings indicate that JAT facilitates ATX degradation via ubiquitination rather via autophagy inhibition. Moreover, the ATX–LPA–LPAR axis has been implicated in the progression of various cancers, including pancreatic ductal adenocarcinoma (PDAC), cholangiocarcinoma (CCA), prostate cancer (PC), and hepatocellular carcinoma (HCC). Consequently, inhibitors and antagonists targeting LPA and its receptors hold promise for cancer therapy. Research on ATX and the development of ATX inhibitors

have become a focus in recent years[36]. Current ATX inhibitors include PF-8380, a piperazinylbenzoxazolone derivative discovered and optimized by Pfizer through compound-library screening[37], and ONO-8430506, a potent tetrahydrocarboline derivative currently under development by Ono Pharmaceuticals Ltd. (Osaka, Japan) [38]. In summary, our study revealed that JAT is an effective inhibitor of the ATX-LPA-LPAR2 pathway.

This study has some limitations. First, whether the most pronounced body weight loss observed in HFD-fed, CRC model mice during DSS water consumption is associated with cancer cachexia was been thoroughly investigated. Second, the metabolic differences between MCM and PCM in cellular models remain unclear. Therefore, these aspects will be further investigated in subsequent studies.

## 5 Conclusions

In both the intestinal tissue of HFD-associated CRC model mice and CT26 cells exposed to an adipocyte-enriched microenvironment, the expression of ATX—a key enzyme for generating bioactive LPA—was elevated. ATX catalyses the conversion of extracellular LPC to LPA, leading to a marked increase in LPA levels in mouse serum and CT26 cell supernatant. Subsequently, LPA, acting as a ligand for LPAR2, upregulates LPAR2 expression in intestinal cells and CT26 cells. As a G protein-coupled receptor (GPCR), LPAR2 activates MAPK signalling upon binding to LPA, thereby promoting tumour cell proliferation and migration.JAT downregulates ATX expression via the UPS, partially by suppressing LPA production. A reduction in LPA expression significantly decreased LPAR2 expression, weakened the LPA-LPAR2 interaction and consequently inhibited the activation of the downstream MAPK pathway, thereby effectively blocking the ATX-LPA-LPAR2-MAPK signalling axis. This mechanism partially corrects the aberrant GPL metabolism in HFD-associated CRC model mice and in CT26 cells under adipocyte-enriched conditions, ultimately suppressing the progression of HFD-related CRC and adipocyte microenvironment-stimulated CRC.In summary, both the in vivo and in vitro findings indicate that a HFD promotes the initiation and progression of CRC and leads to a poor prognosis by activating the ATX-LPA-LPAR2-MAPK axis in the context of GPL metabolism. Although JAT does not directly affect tumour cells, it can inhibit the development of HFD-associated CRC by interfering with tumour metabolic

reprogramming and blocking the ATX-LPA-LPAR2-MAPK signalling axis (Figure 8).

## Ethics approval and consent to participate

All animal handling was performed in accordance with the guidelines established by the National Institute of Animal Care and approved by the Animal Experimentation Ethics Committee -Nanjing University of Chinese Medicine with the protocol approval code of(202404A07).

## Consent for publication

All authors have read and approved the final manuscript for publication. This study does not contain any individual person's data, identifiable images, or videos. No human participants were directly involved in this research; all experiments were performed using commercially available cell lines (HCT116, HT29, CT26), 3T3-L1 adipocytes, and C57BL/6 mice obtained from Commercial company. Therefore, consent for publication from individual persons is not applicable.

## Funding

Jiangsu Provincial Natural Science Foundation Project (BK20201400);
National Famous TCM Expert Liu Shenlin Studio Project of the National Administration of Traditional Chinese Medicine (Document No.: Guozhongyiyaoban Renjiaohan [2018] No. 119);
Jiangsu Universities Advantaged Discipline Construction Project (Document No.: Suzhengbanfa [2018] No. 87).

## Availability of data and materials

The data that support the findings of this study are available from the corresponding author upon reasonable request.

## Acknowledgments

This work was supported by Jiangsu Provincial Natural Science Foundation Project (BK20201400);
National Famous TCM Expert Liu Shenlin Studio Project of the National Administration of Traditional Chinese Medicine (Document No.: Guozhongyiyaoban Renjiaohan [2018] No. 119);
Jiangsu Universities Advantaged Discipline Construction Project (Document No.: Suzhengbanfa [2018] No. 87).

## References


1. Ferlay, J.; Ervik, M.; Lam, F.; Colombet, M.; Mery, L.; Piñeros, M.; Znaor, A.; Soerjomataram, I.; Bray, F. Global Cancer Observatory: Cancer Today. Available online: https://gco.iarc.fr/today (accessed on 10 October 2023).

2. Douaiher J, Ravipati A, Grams B, Chowdhury S, Alatise O, Are C. Colorectal cancer-global burden, trends, and geographical variations. J Surg Oncol. 2017;115:619–30. https://doi.org/10.1002/jso.24578

3. F V, S L, G S, A V, G L. Dietary Factors Modulating Colorectal Carcinogenesis. Nutrients [Internet]. Nutrients; 2021 [cited 2025 Sept 24];13. https://doi.org/10.3390/nu13010143

4. Clinton SK, Giovannucci EL, Hursting SD. The World Cancer Research Fund/American Institute for Cancer Research Third Expert Report on Diet, Nutrition, Physical Activity, and Cancer: Impact and Future Directions. J Nutr. 2020;150:663–71. https://doi.org/10.1093/jn/nxz268

5. Mc R, S O, M KM, Bl E, M V-G, A M, et al. Diet changes due to urbanization in South Africa are linked to microbiome and metabolome signatures of Westernization and colorectal cancer. Nature communications [Internet]. Nat Commun; 2024 [cited 2025 Sept 24];15. https://doi.org/10.1038/s41467-024-46265-0

6. Medina Evora G, Brauer M, Letellier E. Host and microbiome lipid metabolism in colorectal cancer development and therapy. Trends Cancer. 2025;S2405-8033(25)00203-1. https://doi.org/10.1016/j.trecan.2025.08.005

7. Rolle J, Asante DO, Kok-Fong LL, Boucetta H, Seidu TA, Tai LLK, et al. Jatrorrhizine: a review of its pharmacological effects. J Pharm Pharmacol. 2021;73:709–19. https://doi.org/10.1093/jpp/rgaa065

8. Zhong F, Chen Y, Chen J, Liao H, Li Y, Ma Y. Jatrorrhizine: A Review of Sources, Pharmacology, Pharmacokinetics and Toxicity. Front Pharmacol. 2021;12:783127. https://doi.org/10.3389/fphar.2021.783127

9. Kim JI, Huh JY, Sohn JH, Choe SS, Lee YS, Lim CY, et al. Lipid-Overloaded Enlarged Adipocytes Provoke Insulin Resistance Independent of Inflammatiom. Mol Cell Biol. 2015;35:1686–99. https://doi.org/10.1128/MCB.01321-14

10. Lhm G, Tcls S, Rfd A, Accd F, C G, Fa M, et al. Role of lysophosphatidic acid and its receptors in health and disease: novel therapeutic strategies. Signal transduction and targeted therapy [Internet]. Signal Transduct Target Ther; 2021 [cited 2025 Jan 9];6. https://doi.org/10.1038/s41392-020-00367-5

11. Kumar A, Chinnathambi S, Kumar M, Pandian GN. Food Intake and Colorectal Cancer. Nutr Cancer. 2023;75:1710–42. https://doi.org/10.1080/01635581.2023.2242103

12. Zheng S, Yin J, Yue H, Li L. Maternal high-fat diet increases the susceptibility of offspring to colorectal cancer via the activation of intestinal inflammation. Front Nutr. 2023;10:1191206. https://doi.org/10.3389/fnut.2023.1191206

13. Jones AN, Scheurlen KM, Macleod A, Simon HL, Galandiuk S. Obesity and Inflammatory Factors in the Progression of Early-Onset Colorectal Cancer. Cancers (Basel). 2024;16:1403. https://doi.org/10.3390/cancers16071403

14. Miranda BCJ, Tustumi F, Nakamura ET, Shimanoe VH, Kikawa D, Waisberg J. Obesity and Colorectal Cancer: A Narrative Review. Medicina (Kaunas). 2024;60:1218. https://doi.org/10.3390/medicina60081218

15. Ma Y, Yang Y, Wang F, Zhang P, Shi C, Zou Y, et al. Obesity and risk of colorectal cancer: a systematic review of prospective studies. PLoS One. 2013;8:e53916. https://doi.org/10.1371/journal.pone.0053916

16. Molecular Understanding and Pharmacological Potency of Plant-Derived Compounds in Colorectal Cancer (CRC): A Critical Analysis and Future Perspectives | Cell Biochemistry and Biophysics [Internet]. [cited 2024 July 8]. https://link.springer.com/article/10.1007/s12013-024-01370-1. Accessed 8 July 2024

17. Sun J, Shi L, Xu F, Sun H, Liu Y, Sun J, et al. Naringenin Inhibits Colorectal Cancer associated with a High-Fat Diet through Modulation of Gut Microbiota and IL-6/STAT3 Pathway. J Microbiol Biotechnol. 2025;35:e2412029. https://doi.org/10.4014/jmb.2412.12029

18. Pei Y, Song Y, Wang B, Lin C, Yang Y, Li H, et al. Integrated lipidomics and RNA sequencing analysis reveal novel changes during 3T3-L1 cell adipogenesis. PeerJ. 2022;10:e13417. https://doi.org/10.7717/peerj.13417

19. Morita N, Hosaka T, Kitahara A, Murashima T, Onuma H, Sumitani Y, et al. Novel Mechanisms Modulating Palmitate-Induced Inflammatory Factors in Hypertrophied 3T3-L1 Adipocytes by AMPK. J Diabetes Res. 2018;2018:9256482. https://doi.org/10.1155/2018/9256482

20. Sabatino L, Pancione M, Votino C, Colangelo T, Lupo A, Novellino E, et al. Emerging role of the β-catenin-PPARγ axis in the pathogenesis of colorectal cancer. World J Gastroenterol. 2014;20:7137–51. https://doi.org/10.3748/wjg.v20.i23.7137

21. Xiang W, Cheng S, Zhou Y, Ma L. Effects of 1,25(OH)2 D3 on lipid droplet growth in adipocytes. Biofactors. 2020;46:943–54. https://doi.org/10.1002/biof.1610

22. Gonzalez-Baro MR, Coleman RA. Mitochondrial acyltransferases and glycerophospholipid metabolism. Biochim Biophys Acta Mol Cell Biol Lipids. 2017;1862:49–55. https://doi.org/10.1016/j.bbalip.2016.06.023

23. Chen H, Ye C, Wu C, Zhang J, Xu L, Wang X, et al. Berberine inhibits high fat diet-associated colorectal cancer through modulation of the gut microbiota-mediated

663 lysophosphatidylcholine. Int J Biol Sci. 2023;19:2097–113. https://doi.org/10.7150/ijbs.81824

664 24. Law S-H, Chan M-L, Marathe GK, Parveen F, Chen C-H, Ke L-Y. An Updated Review of
665 Lysophosphatidylcholine Metabolism in Human Diseases. Int J Mol Sci. 2019;20:1149.
666 https://doi.org/10.3390/ijms20051149

667 25. Tigyi GJ, Yue J, Norman DD, Szabo E, Balogh A, Balazs L, et al. Regulation of tumor cell -
668 Microenvironment interaction by the autotaxin-lysophosphatidic acid receptor axis. Adv Biol
669 Regul. 2019;71:183–93. https://doi.org/10.1016/j.jbior.2018.09.008

670 26. Yan J, Duan W, Gao Q, Mao T, Wang M, Duan J, et al. ENPP2 inhibitor improves
671 proliferation in AOM/DSS-induced colorectal cancer mice via remodeling the gut barrier
672 function and gut microbiota composition. Pharmacol Res. 2023;195:106877.
673 https://doi.org/10.1016/j.phrs.2023.106877

674 27. Shi W, Peng K, Yu H, Wang Z, Xia S, Xiao S, et al. Autotaxin (ATX) inhibits autophagy
675 leading to exaggerated disruption of intestinal epithelial barrier in colitis. Biochim Biophys
676 Acta Mol Basis Dis. 2023;1869:166647. https://doi.org/10.1016/j.bbadis.2023.166647

677 28. Koike S, Keino-Masu K, Ohto T, Masu M. The N-terminal hydrophobic sequence of
678 autotaxin (ENPP2) functions as a signal peptide. Genes Cells. 2006;11:133–42.
679 https://doi.org/10.1111/j.1365-2443.2006.00924.x

680 29. Takai M, Mori S, Honoki K, Tsujiuchi T. Roles of lysophosphatidic acid (LPA) receptor-
681 mediated signaling in cancer cell biology. J Bioenerg Biomembr. 2024;56:475–82.
682 https://doi.org/10.1007/s10863-024-10028-9

683 30. Chattopadhyay A, Mukherjee P, Sulaiman D, Wang H, Girjalva V, Dorreh N, et al. Role of
684 enterocyte Enpp2 and autotaxin in regulating lipopolysaccharide levels, systemic
685 inflammation, and atherosclerosis. J Lipid Res. 2023;64:100370.
686 https://doi.org/10.1016/j.jlr.2023.100370

687 31. Laface C, Ricci AD, Vallarelli S, Ostuni C, Rizzo A, Ambrogio F, et al. Autotaxin-
688 Lysophosphatidate Axis: Promoter of Cancer Development and Possible Therapeutic
689 Implications. Int J Mol Sci. 2024;25:7737. https://doi.org/10.3390/ijms25147737

690 32. Shida D, Inoue S, Yoshida Y, Kodaka A, Tsuji T, Tsuiji M. Sphingosine kinase 1 is upregulated
691 with lysophosphatidic acid receptor 2 in human colorectal cancer. World J Gastroenterol.
692 2016;22:2503–11. https://doi.org/10.3748/wjg.v22.i8.2503

693 33. Lin S, Lee S-J, Shim H, Chun J, Yun CC. The absence of LPA receptor 2 reduces the
694 tumorigenesis by ApcMin mutation in the intestine. Am J Physiol Gastrointest Liver Physiol.
695 2010;299:G1128-1138. https://doi.org/10.1152/ajpgi.00321.2010

696 34. Sheng X, Yung YC, Chen A, Chun J. Lysophosphatidic acid signalling in development.
697 Development. 2015;142:1390–5. https://doi.org/10.1242/dev.121723

698 35. Wang J, Liu Y, Guo Y, Liu C, Yang Y, Fan X, et al. Function and inhibition of P38 MAP kinase
699 signaling: Targeting multiple inflammation diseases. Biochem Pharmacol. 2024;220:115973.
700 https://doi.org/10.1016/j.bcp.2023.115973

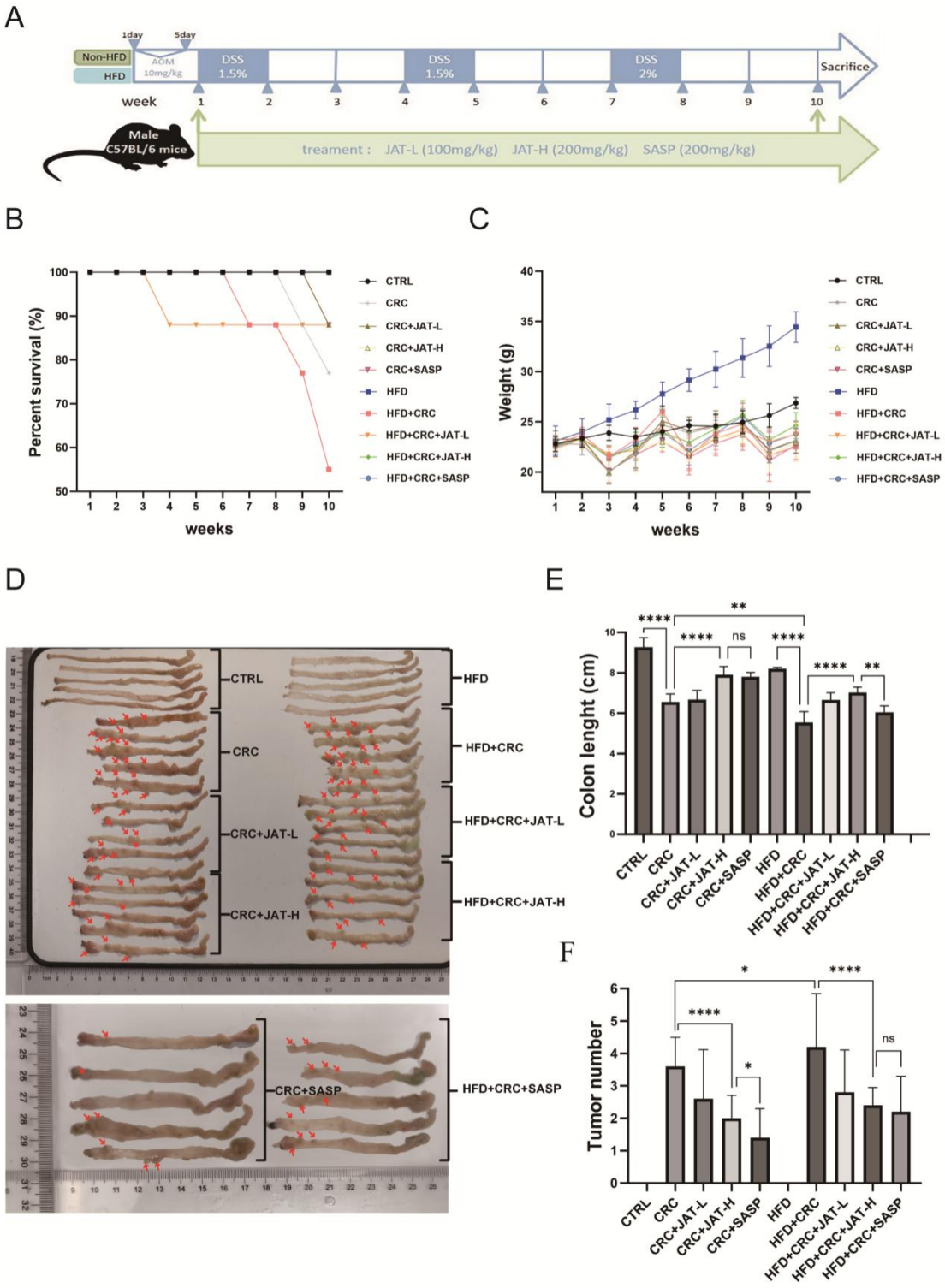
701 36. Zhang C, Liu Y, Zhou Q, Fan H, Liu X, Hu J. Recent research advances in ATX inhibitors: An
702 overview of primary literature. Bioorg Med Chem. 2023;90:117374.
703 https://doi.org/10.1016/j.bmc.2023.117374

704 37. Gierse J, Thorarensen A, Beltey K, Bradshaw-Pierce E, Cortes-Burgos L, Hall T, et al. A novel
705 autotaxin inhibitor reduces lysophosphatidic acid levels in plasma and the site of inflammation.
706 J Pharmacol Exp Ther. 2010;334:310–7. https://doi.org/10.1124/jpet.110.165845

707 38. Saga H, Ohhata A, Hayashi A, Katoh M, Maeda T, Mizuno H, et al. A novel highly potent
708 autotaxin/ENPP2 inhibitor produces prolonged decreases in plasma lysophosphatidic acid
709 formation in vivo and regulates urethral tension. PLoS One. 2014;9:e93230.
710 https://doi.org/10.1371/journal.pone.0093230

711

712 Figure 1




713 **Figure 1.** JAT suppresses HFD-driven colorectal carcinogenesis. (A) Experimental protocol for
714 modelling. (B) Survival rates. (C) Body weight. (D) Representative images of the colon at sacrifice.
715 (E) Colon length. (F) Mean tumour number per animal. $\bar{x}$±s, n=5. The data are presented as the
716 mean ± SD. *p < 0.05, **p < 0.001, ***p < 0.001, ****p < 0.0001.

Figure 2

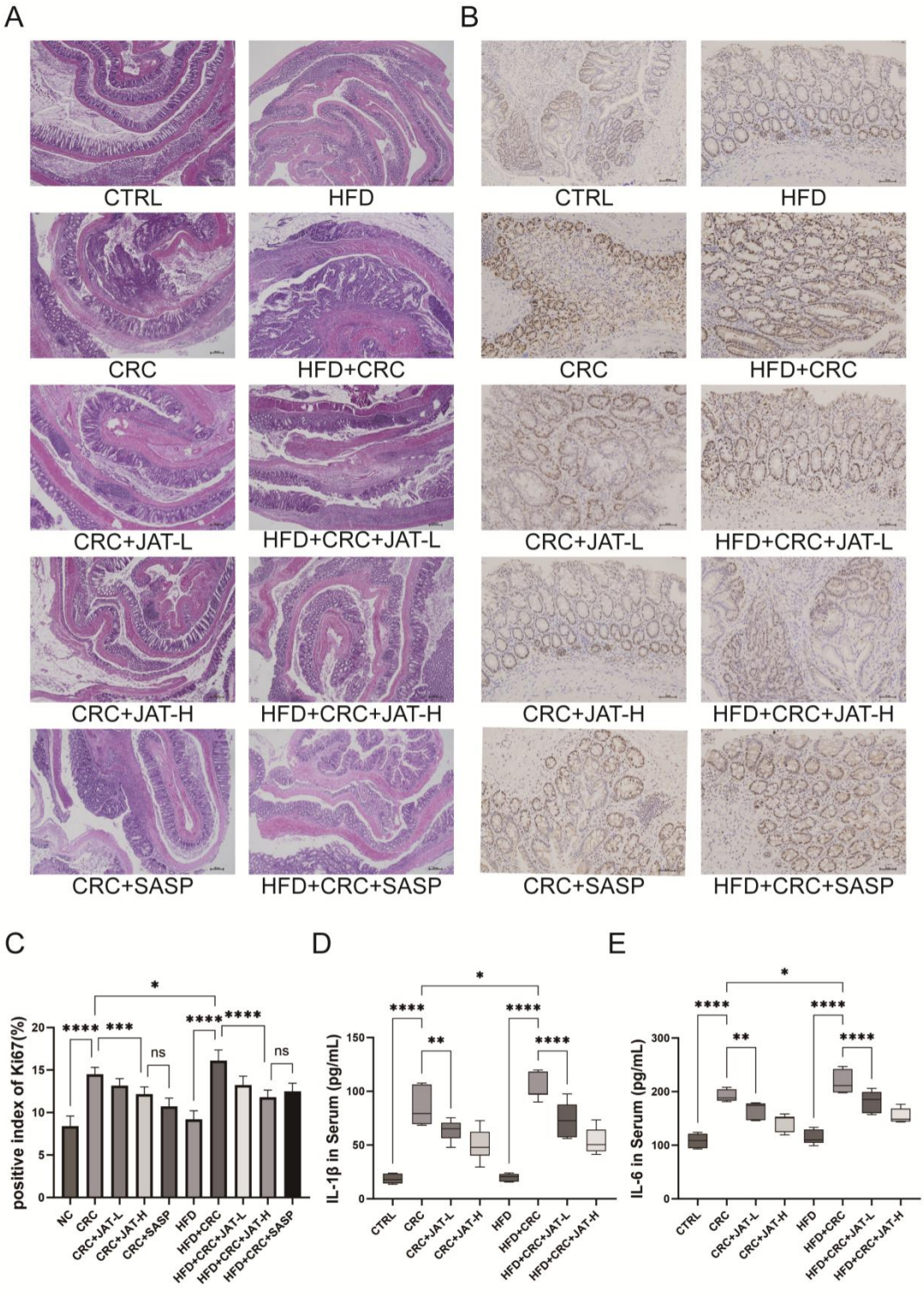



**Figure 2.** JAT suppresses HFD-driven colorectal carcinogenesis. (A) HE staining of intestinal sections. (B) Ki67 IHC staining of colorectal sections. (C) Positive index of Ki67. (D) Serum levels of IL-1β. (D) Serum levels of IL-6. $\bar{x}$±s, n=5. The data are presented as the mean ± SD. *p < 0.05, **p < 0.001, ***p < 0.001, ****p < 0.0001

Figure 3

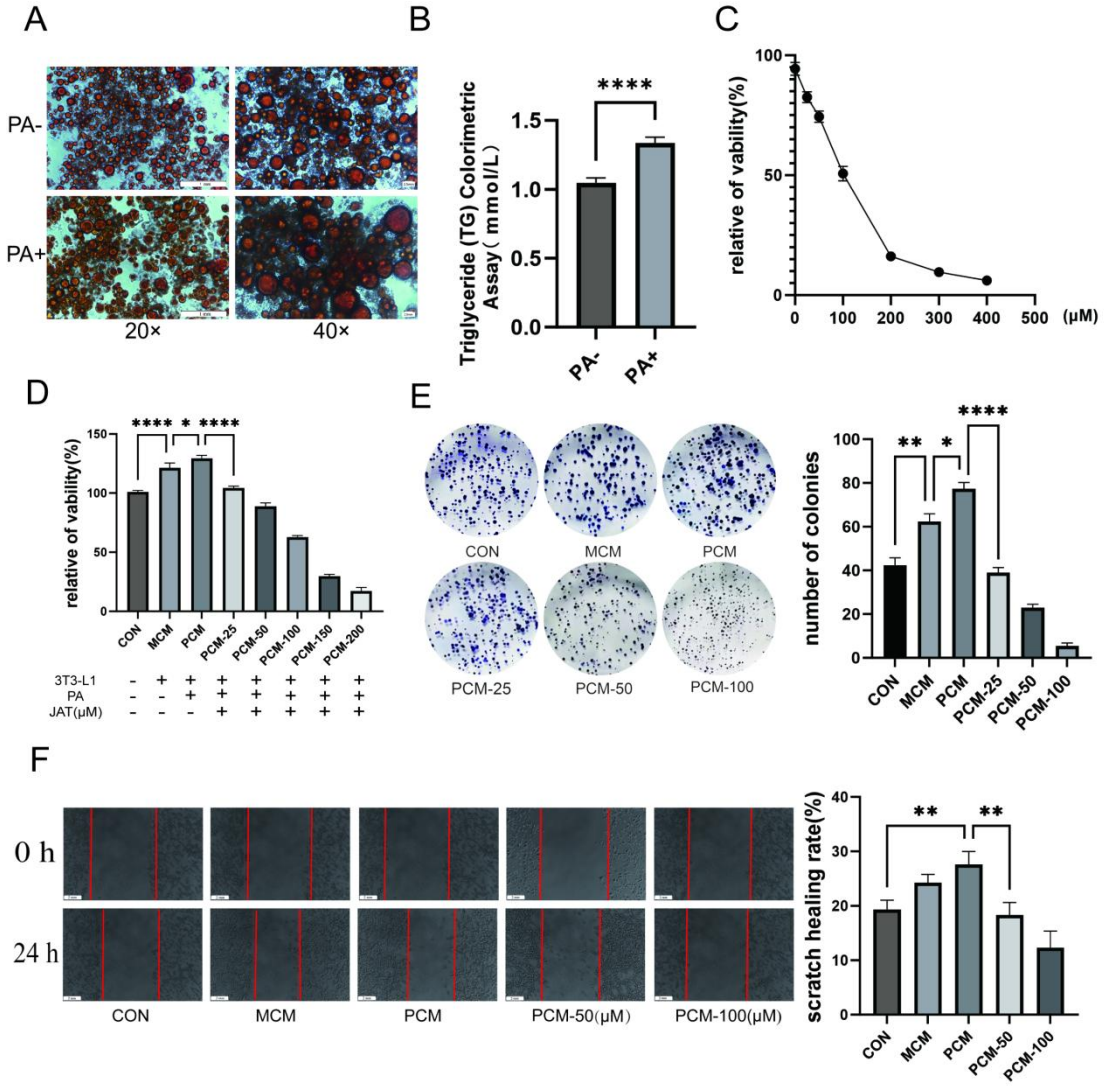
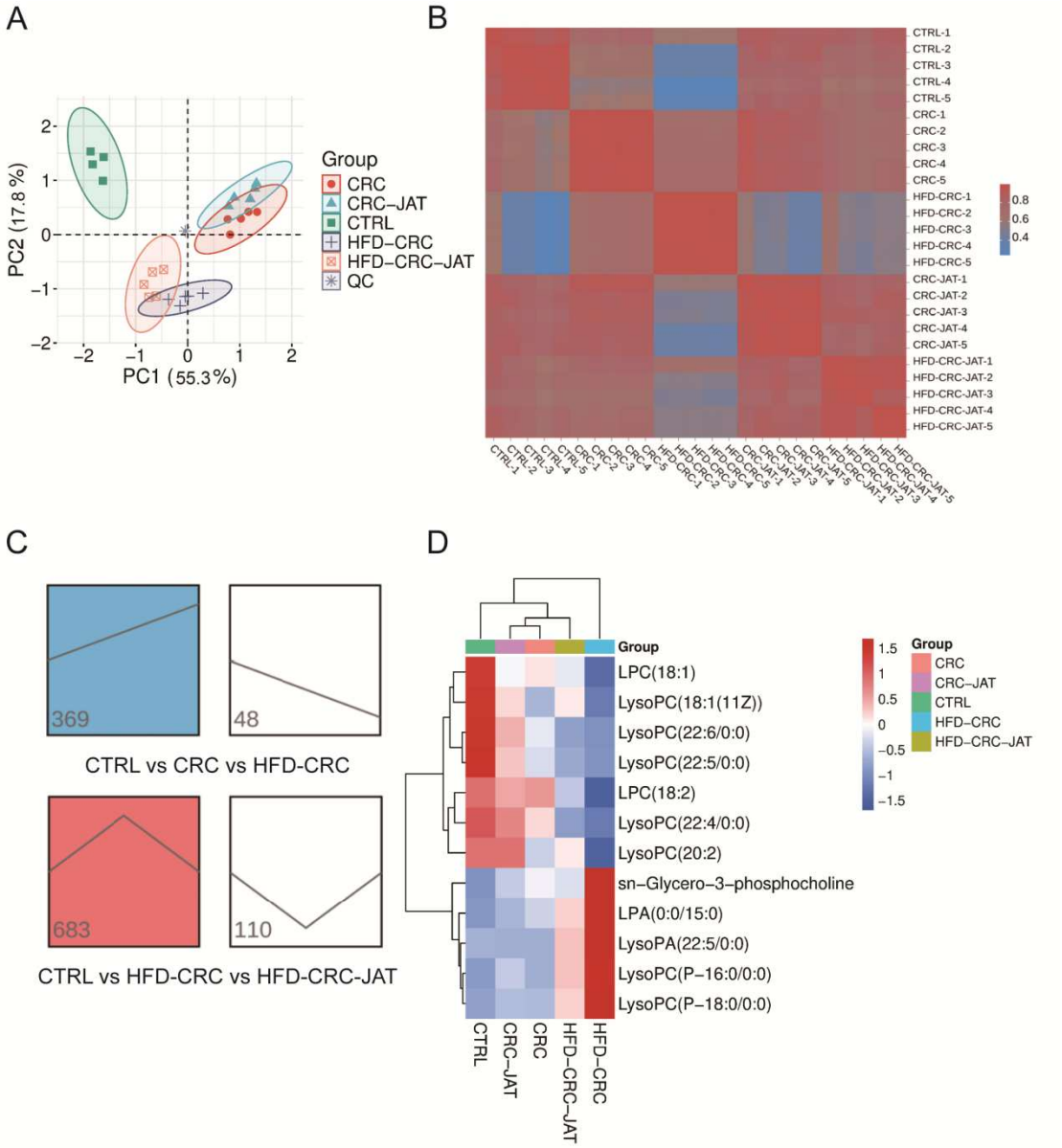



**Figure 3.** Effects of JAT on the Proliferation and Migration of CT26 Cells in an Adipocyte-Conditioned Microenvironment. (A) Differentiation of 3T3-L1 adipocytes. (B) TG content in 3T3-L1 adipocytes determined by a TG colorimetric assay. (C) Effects of JAT on cell viability determined by a CCK-8 assay. (D) CCK-8 assay for assessing group proliferation. (E) Clonogenic assay and analysis. (F) Wound healing assay (10×) and analysis. $\bar{x}$±s, n=3. The data are presented as the mean ± SD. *p < 0.05, **p < 0.001, ***p < 0.001, ****p < 0.0001.

Figure 4


A
PC2 (17.8 %)
PC1 (55.3 %)
Group
CRC
CRC–JAT
CTRL
HFD–CRC
HFD–CRC–JAT
QC
B
CTRL-1
CTRL-2
CTRL-3
CTRL-4
CTRL-5
CRC-1
CRC-2
CRC-3
CRC-4
CRC-5
HFD-CRC-1
HFD-CRC-2
HFD-CRC-3
HFD-CRC-4
HFD-CRC-5
CRC-JAT-1
CRC-JAT-2
CRC-JAT-3
CRC-JAT-4
CRC-JAT-5
HFD-CRC-JAT-1
HFD-CRC-JAT-2
HFD-CRC-JAT-3
HFD-CRC-JAT-4
HFD-CRC-JAT-5
0.8
0.6
0.4
C
369
48
CTRL vs CRC vs HFD-CRC
683
110
CTRL vs HFD-CRC vs HFD-CRC-JAT
D
Group
LPC(18:1)
LysoPC(18:1(11Z))
LysoPC(22:6/0:0)
LysoPC(22:5/0:0)
LPC(18:2)
LysoPC(22:4/0:0)
LysoPC(20:2)
sn–Glycero–3–phosphocholine
LPA(0:0/15:0)
LysoPA(22:5/0:0)
LysoPC(P–16:0/0:0)
LysoPC(P–18:0/0:0)
CTRL
CRC–JAT
CRC
HFD–CRC–JAT
HFD–CRC
1.5
1
0.5
0
−0.5
−1
−1.5
Group
CRC
CRC–JAT
CTRL
HFD–CRC
HFD–CRC–JAT

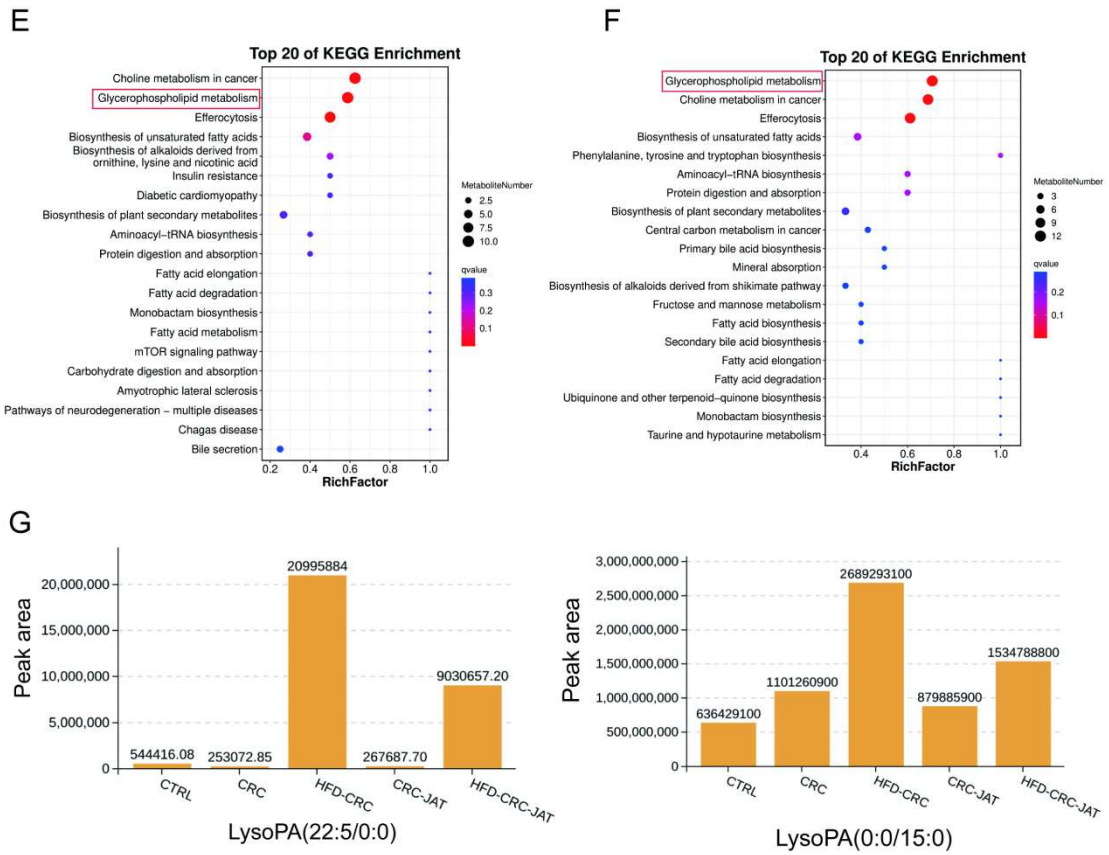



**Figure 4.** Nontargeted metabolomics revealed changes in metabolites in CRC and HFD+CRC model mice following JAT treatment. (A) PCA plot of the groups. (B) Clustered heatmap of intersample correlations. (C) Metabolite trend analysis. (D) GPL metabolite clustering heatmap. (E) CRC vs. HFD+ CRC KEGG pathway enrichment analysis. (F) HFD+CRC vs. HFD+CRC+JAT KEGG pathway enrichment analysis. (G) Differential analysis of lysophosphatidic acid (LPA) metabolites.

Figure 5

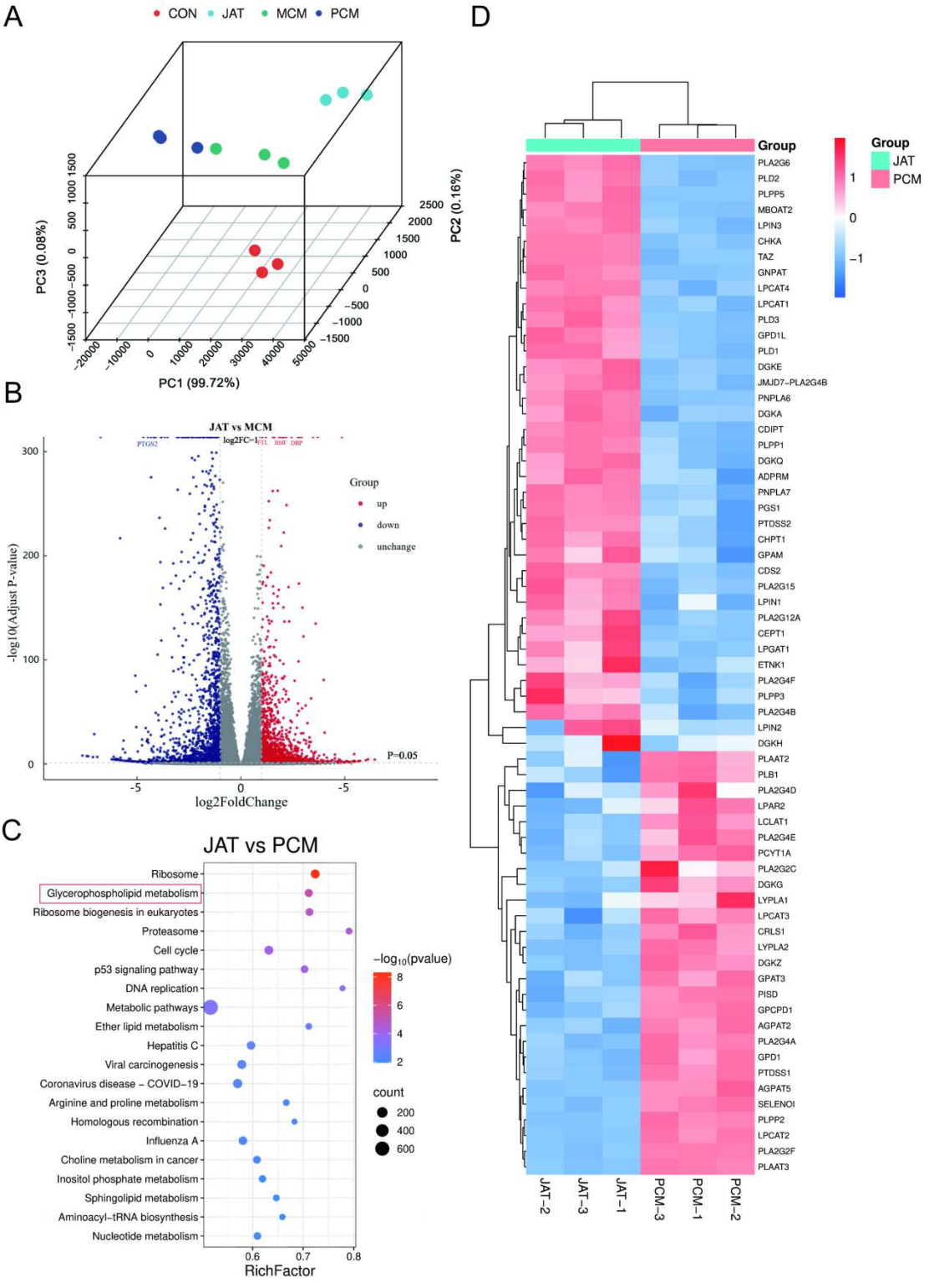
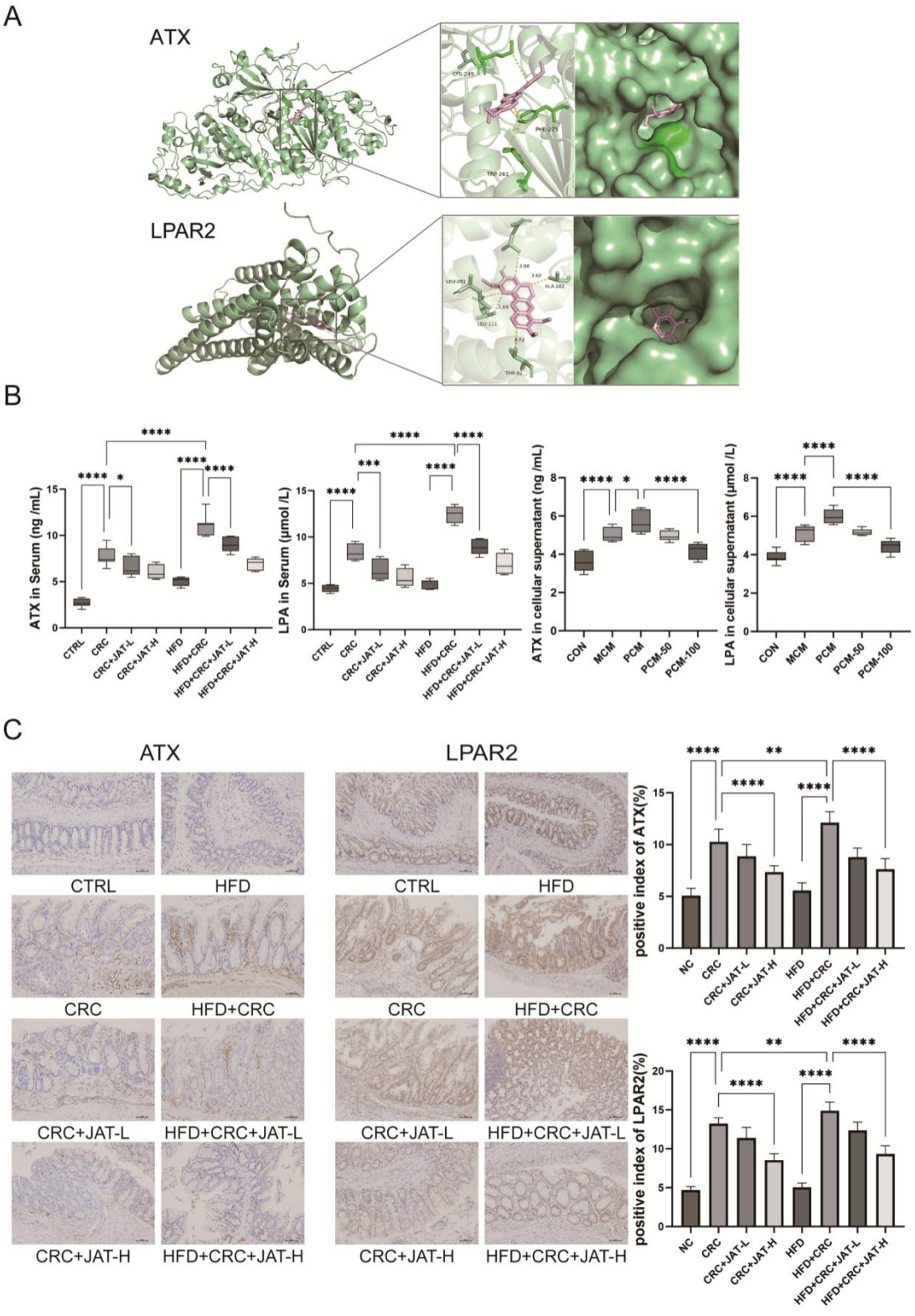



**Figure 5.** Transcriptome sequencing analysis of CT26 cells stimulated by adipokines with JAT intervention. (A) Principal component analysis (PCA) of the transcriptomic variation across the experimental groups. (B) Volcano plot of differentially expressed genes (DEGs) (|log2FC| > 1, p < 0.05). (C) KEGG pathway analysis: JAT vs. PCM. (D) Heatmap of differential gene expression in

the GPL metabolic pathway.

Figure 6



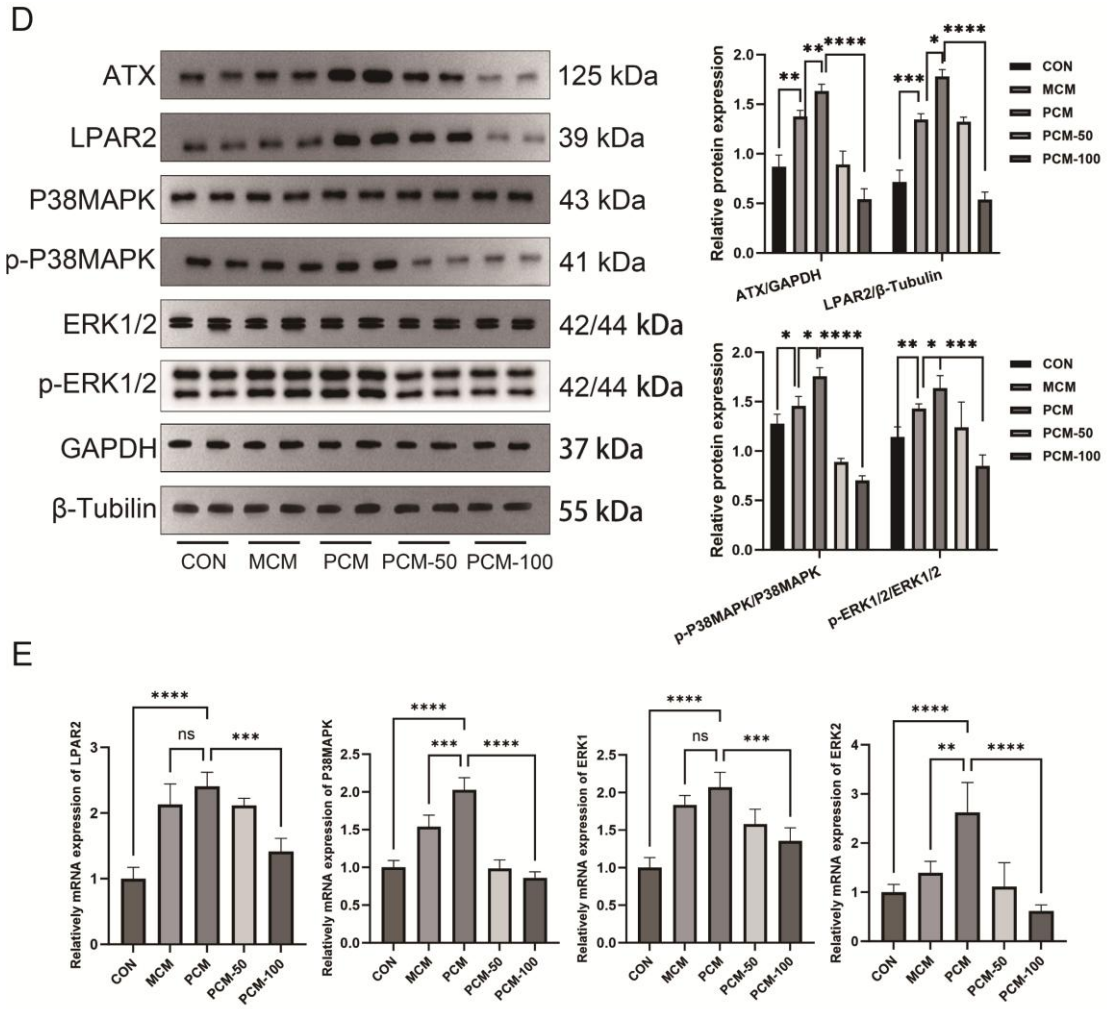
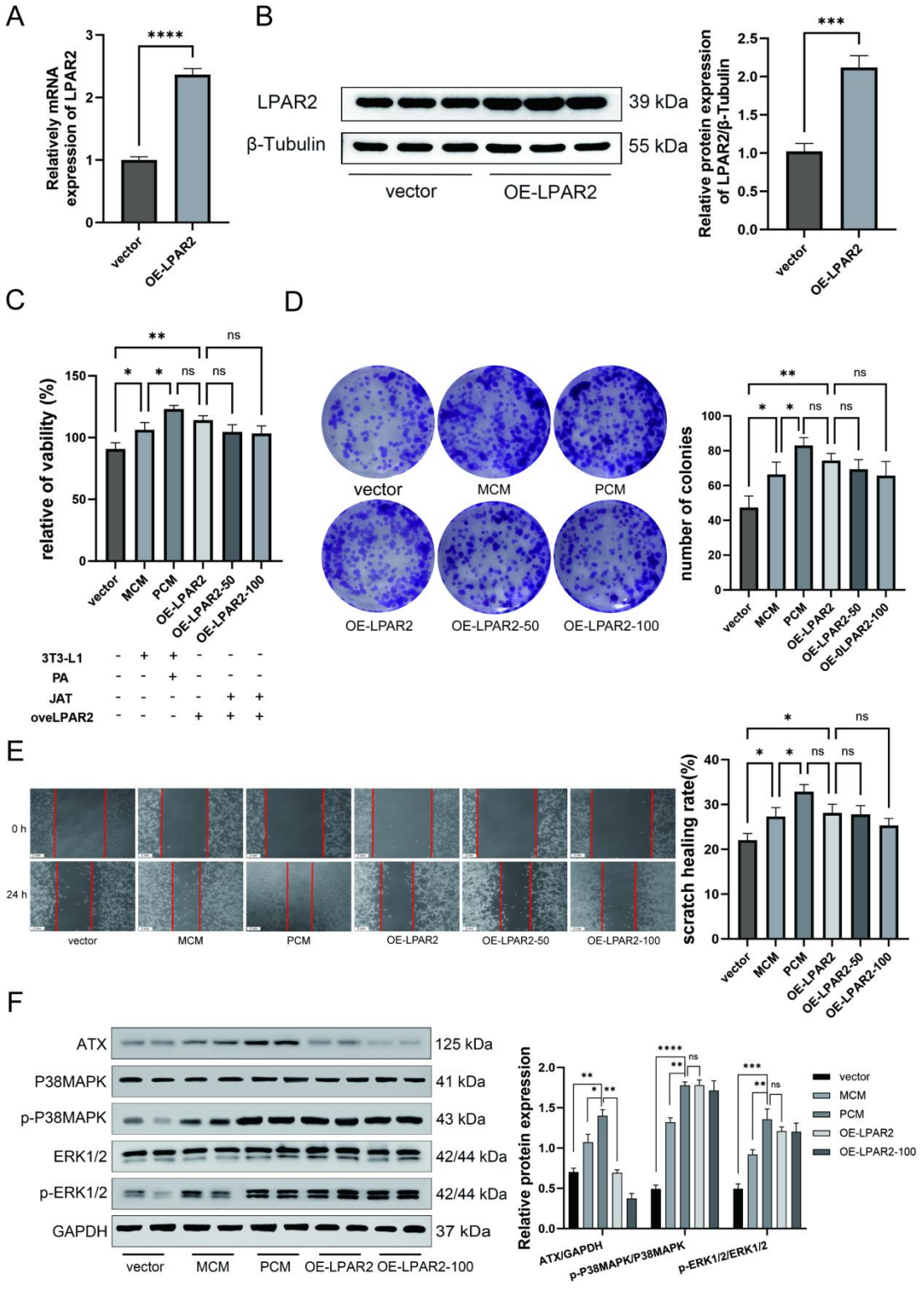



**Figure 6.** A HFD-fed and adipocyte-based environment activates the ATX-LPA-LPAR-MAPK signalling axis in CRC model mice and CT26 cells, whereas JAT inhibits this pathway. (A) Molecular docking poses of JATs within the binding pockets of ATX and LPAR2 proteins. (B) LPA and ATX levels in mouse serum and cell culture supernatants measured by ELISA. (C) IHC analysis of ATX and LPAR2 protein expression in mouse colorectal tissue (positive staining quantified using ImageJ). (D) WB analysis of key proteins in MCM/PCM-cultured CT26 cells treated with JAT (50/100 μmol/L), with band intensities quantified by ImageJ. (E) mRNA expression of key genes in the CON, MCM, PCM, PCM-50, and PCM-100 groups. $\bar{x}$±s, n=3. The data are presented as the mean ± SD. *p < 0.05, **p < 0.001, ***p < 0.001, ****p < 0.0001.

785 Figure 7




786

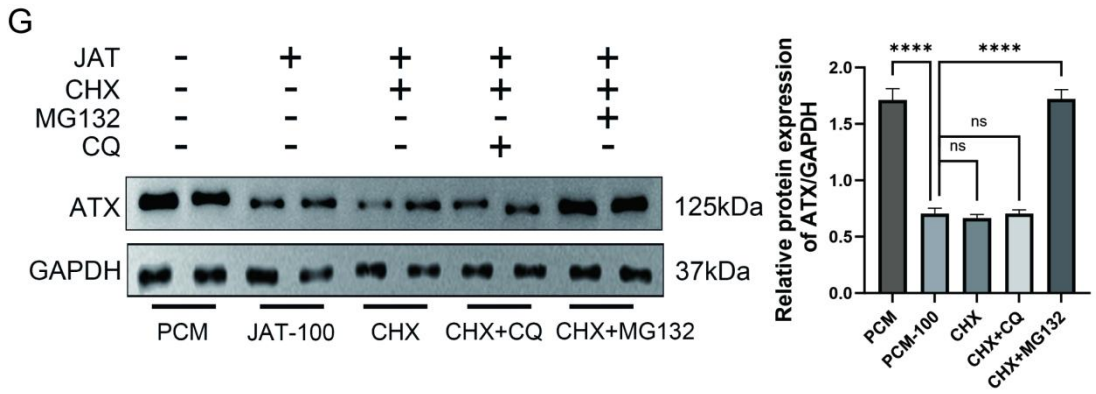



**Figure 7.** JAT inhibits LPAR2-activated MAPK signalling and directly promotes the proteasomal degradation of ATX. (A) Comparison of LPAR2 mRNA expression levels between the LPAR2-overexpressing group (OE-LPAR2) and the vector control group. (B) Comparison of LPAR2 protein expression levels between the OE-LPAR2 group and the vector control group. (C) Cell viability analysed by a CCK-8 assay following LPAR2 overexpression. (D) Proliferative capacity was assessed by a colony formation assay after LPAR2 overexpression. (E) Analysis of cell migration ability via a wound healing assay (10× magnification) after LPAR2 overexpression. (F) WB analysis of ATX, p-p38 MAPK, and p-ERK1/2 protein expression upon LPAR2 overexpression. (G) WB analysis of JAT-induced ATX protein degradation. $\bar{x}$±s, n=3. The data are presented as the mean ± SD. *p < 0.05, **p < 0.001, ***p < 0.001, ****p < 0.0001.

Figure 8

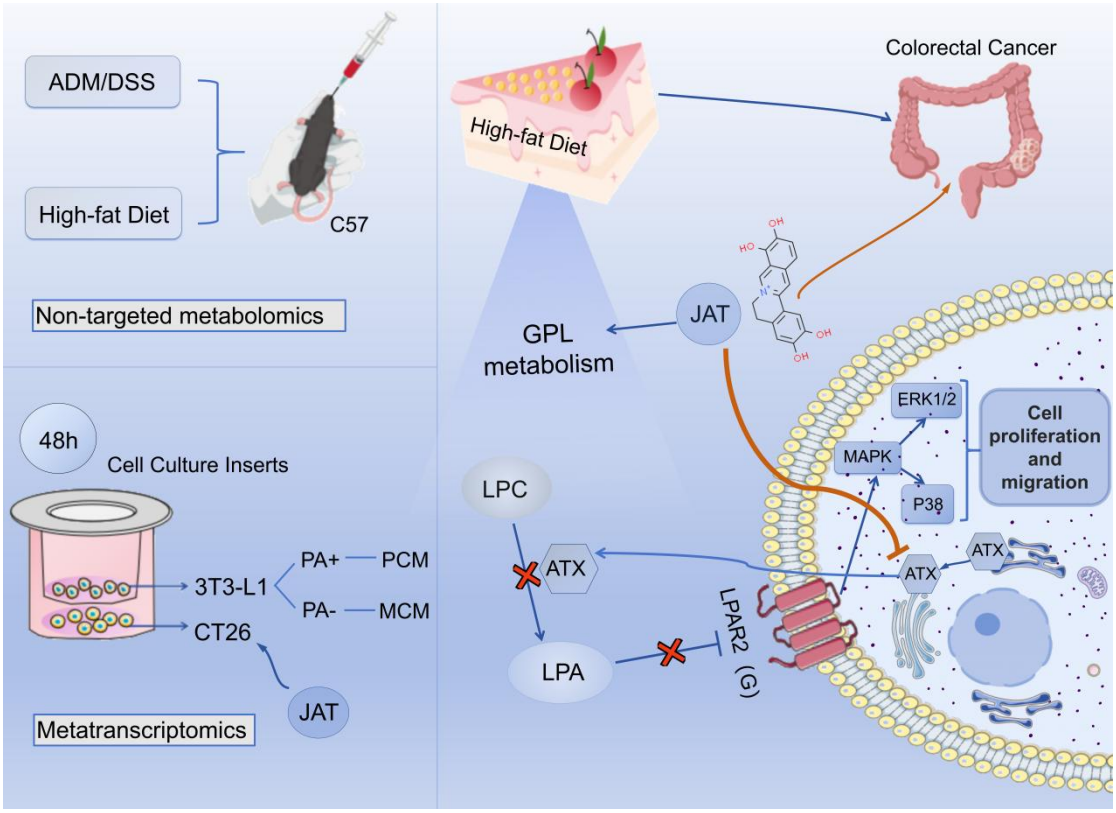



**Figure 8.** Mechanistic diagram of this article.

Using both an HFD-fed AOM/DSS-induced murine CRC model and a 3T3-L1 adipocyte-CT26 CRC cell coculture system, we demonstrated that JAT attenuates HFD-induced colorectal carcinogenesis by suppressing ATX-LPA-LPAR2-MAPK signalling activity and reversing GPL metabolic reprogramming. Mechanistically, JAT inhibits ATX—the rate-limiting enzyme for extracellular LPA secretion by adipose and tumour tissues—thereby reducing LPC-to-LPA conversion. Concurrently, JAT downregulates LPAR2 expression in CRC cells, attenuating LPA-LPAR2 interactions and consequently suppressing the phosphorylation of the downstream effectors p38 MAPK and ERK1/2.

829

## Supplementary Files

This is a list of supplementary files associated with this preprint. Click to download.

- supplementaryMaterialcelltranscriptomeTotalDEGBar.tif